The Journal of Chemical Physics

Ruthenium hydrides encapsulated in sol–gel glasses exhibit new ultrafast vibrational dynamics

Cite as: J. Chem. Phys. **156**, 124502 (2022); https://doi.org/10.1063/5.0082752
Submitted: 17 December 2021 • Accepted: 07 March 2022 • Published Online: 23 March 2022

Cynthia G. Pyles, Joel G. Patrow, Yukun Cheng, et al.

The Journal of Chemical Physics ARTICLE scitation.org/journal/jcp

Ruthenium hydrides encapsulated in sol–gel glasses exhibit new ultrafast vibrational dynamics

Cite as: J. Chem. Phys. 156, 124502 (2022); doi: 10.1063/5.0082752
Submitted: 17 December 2021 • Accepted: 7 March 2022 •
Published Online: 23 March 2022

Cynthia G. Pyles, Joel G. Patrow, Yukun Cheng, Ian A. Tonks, and Aaron M. Massari[a)]

AFFILIATIONS

University of Minnesota–Twin Cities, 207 Pleasant St. SE, Minneapolis, Minnesota 55454, USA

Note: This paper is part of the JCP Special Topic on Time-Resolved Vibrational Spectroscopy.
[a)]**Author to whom correspondence should be addressed:** massari@umn.edu

ABSTRACT

Vibrational dynamics were measured by IR pump–probe spectroscopy and two-dimensional IR spectroscopy for triruthenium dodecacarbonyl and the undecacarbonyl hydride that forms when it is encapsulated in an alumina sol–gel glass. For comparison, a triruthenium undecacarbonyl hydride salt was also synthesized and studied in neat solution to identify the potential influence of the confined solvent environment on the dynamics experienced by carbon monoxide ligands. The vibrational lifetime was found to be significantly decreased for both hydride species relative to the dodecacarbonyl compound. Conversely, spectral diffusion of the CO vibrations was measured to be faster for the parent compound. The most significant dynamic changes occurred upon transformation from the starting compound to the hydride, while only minor differences were observed between the dynamics of the freely dissolved and sol–gel encapsulated hydrides. The results suggest that the structural change to the hydride has the largest impact on the dynamics and that its improved catalytic properties likely do not originate from confined solvent effects.

INTRODUCTION

The dynamics of molecules in the first solvation shell surrounding a catalyst are key to enabling reactants to reach a transition state and form products.[1–4] These time-dependent solvent–solute interactions stabilize or destabilize the transition state, thereby directly influencing the rate coefficient.[5–9] It is for precisely this reason that catalytic rate constants are almost always solvent specific.[10–13] The random, thermally driven motions of solvent molecules effectively allow the catalyst (and substrate) to sample the energetic landscape that spans the reaction coordinate. In biomacromolecules, for example, key structural motions for the reactivity of enzymes have been tied to the dynamics of the surrounding solvation layer.[14–19] Ultrafast dynamics in the solvation shell have also been implicated in mechanistic steps for organometallic catalysts.[20,21]

In addition to changing the identity of the solvent itself, the reactivity of catalysts can also be controlled by encapsulation in small volumes of solvent inside solid support matrices, such as zeolites or sol–gel glasses.[22–26] Alumina sol–gels have been shown to increase the catalytic activity of homogeneous catalysts entrapped inside of the sol–gel pores.[27–29] In a recent study, it was shown that encapsulation of $Ru_3(CO)_{12}$ in alumina sol–gels increased its catalytic activity for hydrogenation reactions.[28] It was proposed that the improved activity originated from the formation of catalytically active metal hydrides during the sol–gel aging process;[29] metal hydrides have a long history in chemical catalysis.[30–32] In a subsequent study, our group demonstrated definitively that the ruthenium hydride $\{[HRu_3(CO)_{11}]^-\}$ was indeed formed within the alumina sol–gel glass with the concomitant loss of a CO ligand;[33] however, we did not explore the role that solvent dynamics in nanoscopic pores might play in the catalytic activity.

To address this question in this study, infrared pump–probe spectroscopy and two-dimensional infrared (2D-IR) spectroscopy were performed on $Ru_3(CO)_{12}$ and $[NEt_4][HRu_3(CO)_{11}]$ in tetrahydrofuran (THF) and $[HRu_3(CO)_{11}]^-$ encapsulated in an alumina sol–gel. We explore how the chemical conversion to a metal hydride and the environmental encapsulation in an alumina sol–gel affect vibrational dynamics reported by the CO ligands.

EXPERIMENTAL

Materials

$Ru_3(CO)_{12}$, aluminum isopropoxide [Al(O-i-Pr)$_3$], and tetrahydrofuran (THF) used for alumina sol–gel studies were purchased from Millipore-Sigma and used as received. Sodium borohydride ($NaBH_4$) used in the air- and moisture-sensitive synthesis of $[NEt_4][HRu_3(CO)_{11}]$ was purchased from Millipore-Sigma and dried *in vacuo* prior to use. The solvents used in the synthesis of $[NEt_4][HRu_3(CO)_{11}]$ (THF, pentane, dichloromethane, and Et_2O) were dried through activated alumina on a Pure Process Technology solvent purification system.

Sol–gel formation

$Ru_3(CO)_{12}$ alumina sol–gels were prepared according to a previous procedure.[28] Approximately 0.02 mmol of $Ru_3(CO)_{12}$ was dissolved in 1 ml of THF and the solution was stirred. Separately, ~6 mmol of Al(O-i-Pr)$_3$ was dissolved in 4 ml of THF, which was then decanted into the stirring $Ru_3(CO)_{12}$ solution. The mixture was stirred for 20 min. For the FTIR, pump–probe, and 2D-IR measurements, the $Ru_3(CO)_{12}$/Al(O-i-Pr)$_3$ mixture was sandwiched between two calcium fluoride (CaF_2) windows with a 50 μm spacer that had two small strips cut out of the spacer (one on top and one at the bottom) to allow for the introduction of water. The sandwiched sol–gel sample was then placed in a homemade solvent cell built in such a way that water surrounded the sample edges. This allowed water to diffuse into the $Ru_3(CO)_{12}$/Al(O-i-Pr)$_3$ mixture and catalyze the alumina sol–gel formation.

Synthesis of $[NEt_4][HRu_3(CO)_{11}]$

In a glovebox, $Ru_3(CO)_{12}$ (106 mg, 0.166 mmol), $NaBH_4$ (33 mg, 0.87 mmol), and 17 ml of THF were added to a 20 ml scintillation vial along with a small stir bar. The reaction vial was then sealed with a Teflon screw cap and stirred for 40 min at room temperature. [Et$_4$N]Br (42 mg, 0.20 mmol) was then added to the solution, and the reaction mixture was stirred for another 1 h. The solution was filtered through a pipet plug and concentrated to 2 ml in vacuum. 15 ml of pentane was added to the solution to form a precipitate. The resulting suspension was filtered and the precipitate was washed with 2 ml of pentane. The precipitate was then dissolved in CH_2Cl_2, and crystallization of $[NEt_4][HRu_3(C)_{11}]$ was achieved by vapor diffusion of Et_2O into CH_2Cl_2, yielding $[NEt_4][HRu_3(C)_{11}]$ as reddish-brown crystals. The final yield was 95 mg (0.13 mmol, 77%). For characterization details, see Ref. 33.

FTIR measurements

All FTIR spectra were collected using a Nicolet 6700 FTIR spectrometer (Thermo Scientific). The resolution was 1 cm^{-1} at 16 scans. The spectrum of $Ru_3(CO)_{12}$ in THF was collected with THF as the background. The spectra of $Ru_3(CO)_{12}$ entrapped in the alumina sol–gel were collected with air as the background. In cases where "ultradry THF" was used for spectroscopy, THF was taken from a Pure Process Technology solvent purification system and stored over 4 Å sieves in a glovebox. Solvent dryness was measured through a Na/Ph_2CO ketyl radical titration, with a maximum threshold of ~10 ppm H_2O.

2D-IR measurements

The 2D-IR setup has been described previously.[8,9] Briefly, a regeneratively amplified Ti:sapphire laser (Spectra-Physics, 800 nm, 40 fs pulse duration FWHM, 30 nm bandwidth FWHM, 600 mW) pumped an optical parametric amplifier (OPA) (Spectra-Physics) with a repetition rate of 1 kHz. The near-IR signal and idler beams generated by the OPA's β-barium borate (BBO, 3 mm thick) crystal were difference frequency mixed in a silver gallium sulfide crystal ($AgGaS_2$, 0.5 mm thick), generating 3 μJ mid-IR pulses. The final output pulses had a spectrum that was centered at 2040 cm^{-1} (THF sample) or 2020 cm^{-1} (sol–gel sample). The bandwidth was ~200 cm^{-1} (FWHM). The mid-IR pulse train was split into three separate beams and focused onto the sample in the BOXCARS geometry.[10] The generated vibrational echo was overlapped with a local oscillator and sent to a spectrometer with a spectral resolution of 4 cm^{-1} and detected with a liquid nitrogen cooled 64-pixel mercury cadmium telluride (MCT) linear array detector (Infrared Associates, Inc.). The entire mid-IR beam path was purged with dry air (−100 °F dew point).

RESULTS AND DISCUSSION

The FTIR spectrum of $Ru_3(CO)_{12}$ in THF shows three strong peaks at 2005, 2030, and 2060 cm^{-1} (Fig. 1). These peaks have been assigned as the E′ (radial), A_2' (axial), and E′ (axial) carbonyl modes on the ruthenium molecule.[33–36] Sol–gel formation results in the complex losing one carbon monoxide ligand. Drastic changes to the spectral changes occur with new peaks at 1951, 1961, 1987, and 2014 cm^{-1}. The synthesized version of the hydride, $[NEt_4][HRu_3(CO)_{11}]$, has an FTIR spectrum that is identical to that of the sol–gel (Fig. 1), confirming the formation of a hydride within the nanoscopic alumina pores.

One way that encapsulation could affect catalyst reactivity is by perturbing the coupling to the solvent bath, which then impacts

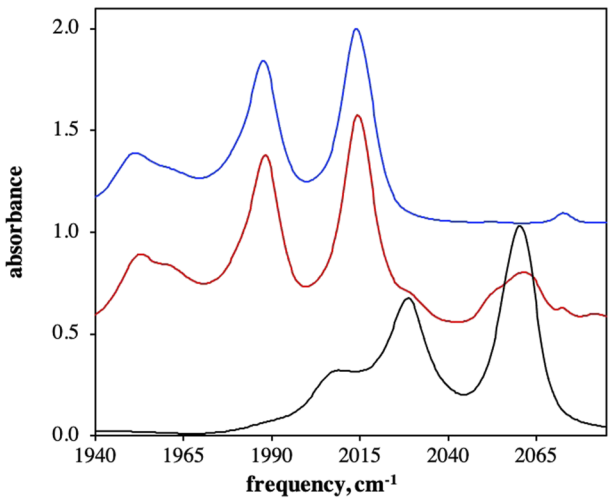

FIG. 1. Normalized FTIR spectra of $Ru_3(CO)_{12}$ in THF (black), converted $[HRu_3(CO)_{11}]^-$ encapsulated in an alumina sol–gel glass (red), and $[NEt_4][HRu_3(CO)_{11}]$ dissolved in THF (blue). Spectra are offset for clarity.

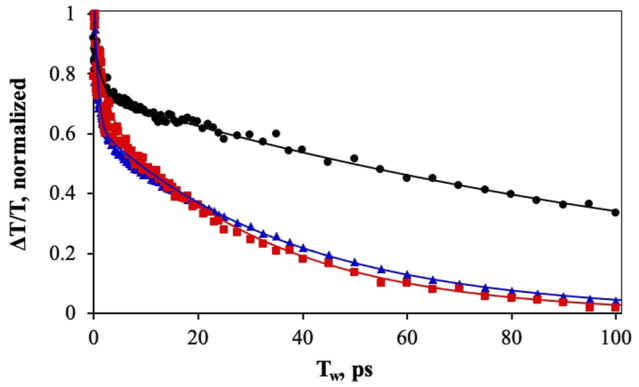

FIG. 2. IR pump–probe population decay for the high frequency carbonyl stretch of $Ru_3(CO)_{12}$ in THF (black circles), $[HRu_3(CO)_{11}]^-$ in the alumina sol–gel (red squares), and $[NEt_4][HRu_3(CO)_{11}]$ in THF (blue triangles). The markers represent the experimental data, and the solid lines show the biexponential fit.

the rate of vibrational energy relaxation (VER).[37–41] We performed IR pump–probe measurements to compare the relaxation dynamics of $Ru_3(CO)_{12}$ in THF, $[HRu_3(CO)_{11}]^-$ in an alumina sol–gel glass, and $[NEt_4][HRu_3(CO)_{11}]$ in THF. The congested nature of the FTIR spectra in Fig. 1 led to convoluted pump–probe spectra for all three samples. To avoid artifacts, the blue edges of the highest energy carbonyl modes (~2065 or ~2019 cm^{-1}) in the pump–probe spectra were analyzed.

Selected population decays for all three samples were fit to biexponential decay functions as shown in Fig. 2 (fit parameters tabulated in Table S1). The fast time constants are on the order of 1 ps in all cases, and we attribute this to fast intramolecular redistribution (IVR). This was confirmed by directly measuring IVR occurring on the same time scale by analyzing the 2D-IR spectra as shown in the supplementary material (Fig. S1). The most salient difference between the dynamics in Fig. 2 is that $[HRu_3(CO)_{11}]^-$ in the sol–gel (T_1 = 30 ± 8 ps) and in THF (T_1 = 37 ± 2 ps) exhibits drastically shorter lifetimes than $Ru_3(CO)_{12}$ (T_1 = 144 ± 15 ps). This difference suggests that the hydride (encapsulated or synthesized) couples to its environment differently than $Ru_3(CO)_{12}$. This difference cannot be attributed to small amounts of water that are formed by alumina hydrolysis during sol–gel synthesis since both $Ru_3(CO)_{12}$ and synthesized $[HRu_3(CO)_{11}]^-$ were measured in ultradry THF and still reflect this difference. We have previously shown that the formation of the hydride places additional electron density on the Ru nuclei. The Ru nuclei then participate in π-backbonding and place additional electron density on the carbonyl ligands, which shift their vibrational frequencies.[33] A shift in vibrational frequency can allow for better energy-match between the solvent and the solute vibrational modes, which would expedite VER. For example, THF has a weak mode at 1980 cm^{-1} that would be in registry with the red-shifted hydride spectra and may provide this pathway.

On the other hand, the comparison of VER between the two hydrides in this study also reveals smaller differences: The carbonyl mode encapsulated by the sol–gel relaxes 7 ps faster than the same mode in ultradry THF. Although the majority of the solvent in the pores has been exchanged with THF, there is certainly some residual water in this sample that impacts VER for the CO modes. We showed that adding water to a $Ru_3(CO)_{12}$ in THF solution, for example, can lower the lifetime by about 75%, which is consistent with the decrease between the two hydrides (Fig. S2 and Table S1). Modified THF bath modes inside the sol–gel pores, newly formed low-lying energy-accepting modes among the alumina sol–gel matrix, or finite amounts of water in the pores could all provide alternate mechanisms of VER that expedite vibrational relaxation. The similarity in T_1 values for the synthesized hydride in dry THF and sol–gel encapsulated hydride provides indirect evidence that the pores contain predominantly THF. Nonetheless, residual water cannot explain the acceleration in relaxation from $Ru_3(CO)_{12}$ to $[HRu_3(CO)_{11}]^-$. We find that even adding copious amounts of water (1:5 H_2O:THF) to the $Ru_3(CO)_{12}$ solution is only able to lower the CO lifetime to 110 ps (Table S1).

The solvent dynamics of the three compounds were further studied via 2D-IR spectroscopy. The representative 2D-IR spectra are shown in Fig. 3 for $Ru_3(CO)_{12}$ in ultradry THF, alumina sol–gel, and $[NEt_4][HRu_3(CO)_{11}]$ in ultradry THF at short (0.5 ps) and long

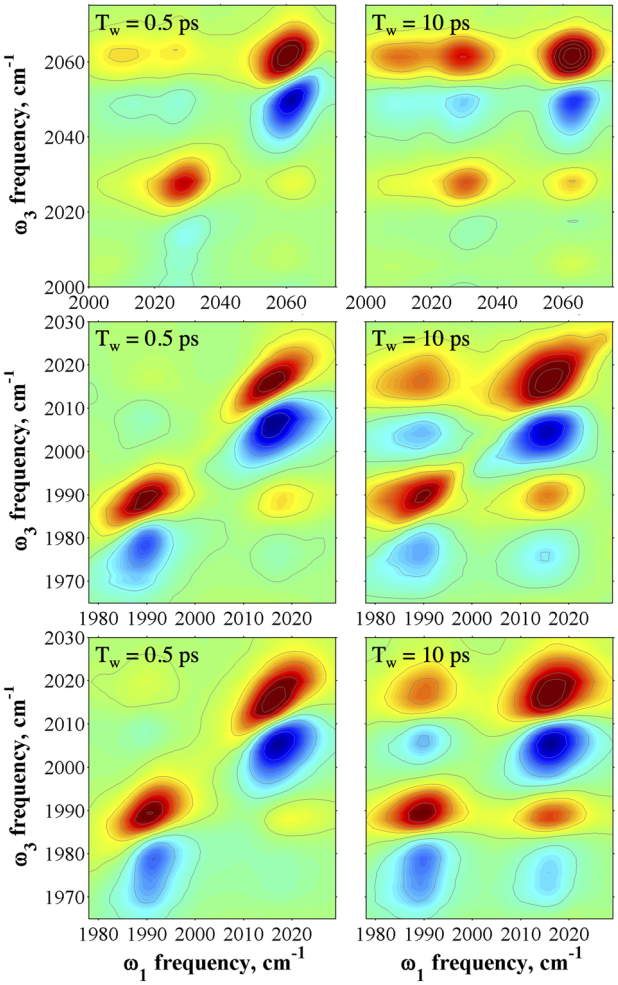

FIG. 3. 2D-IR spectra of $Ru_3(CO)_{12}$ in THF (top row), alumina sol–gel (middle row), and $[Net_4][Hru_3(CO)_{11}]$ in THF (bottom row) at 0.5 ps (left) and 10 ps (right).

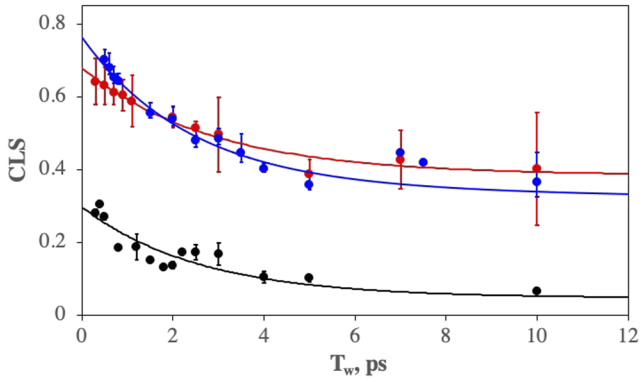

FIG. 4. CLS as a function of T_w for the 2060 cm^{-1} mode in $Ru_3(CO)_{12}$ in ultradry THF (black) and the 2014 cm^{-1} mode for $[HRu_3(CO)_{11}]^-$ in the alumina sol–gel (red) and in ultradry THF (blue).

(10 ps) waiting times (T_w). The x axes of the 2D-IR spectra are the pump frequencies (ω_1) and the y axes are the probe frequencies (ω_3). The red peaks arise from the ground state bleach of the $v = 1 \rightarrow 0$ transition, while the blue peaks arise from the $v = 1 \rightarrow 2$ excited state absorption. All spectra show strong on-diagonal peaks corresponding to the peaks in the FTIR spectra in Fig. 1 as well as off-diagonal peaks that grow as T_w is increased. The off-diagonal peaks indicate the exchange of excitation between modes that are coupled.

The 2D-IR line shapes change with T_w for all three systems. At early T_ws, the spectra are elongated along the $\omega_3 = \omega_1$ diagonal. At later T_ws, the peaks become increasingly round. Qualitatively, the vibrational modes in $Ru_3(CO)_{12}$ appear to have experienced more spectral diffusion over the first 10 ps than either of the hydride species. Spectral diffusion refers to the process by which vibrational frequencies are modified by structural changes and movements of the solute and nearby solvent molecules. The dynamics were quantified as a function of T_w via the center line slope (CLS) method.[42] A plot of the CLS values as a function of waiting time (T_w) is shown in Fig. 4. CLS values for the Ru_3CO_{12} and $[NEt_4][HRu_3(CO)_{11}]$ samples in ultradry THF were obtained out to 70 ps. The shorter vibrational lifetime and heterogeneous nature of the sol–gel sample lead to increased scatter and worse signal to noise, even with the use of scattering cancellation techniques,[43] thereby limiting the T_w range to under 20 ps.

For clarity, we focus our analysis here on the 2060 and 2014 cm^{-1} modes for $Ru_3(CO)_{12}$ and the hydride species, respectively, since these avoid overlapping with other spectral features. Each CLS decay was fit to an exponential decay plus a constant offset. The time constants for the fast component of the biexponential decays (τ_1) are the same within errors (Table I) and are all near 3 ps. Hence, the frequency fluctuations experienced by the CO ligands due to their surroundings for the Ru_3CO_{12} and hydride compounds occur on similar time scales. The alumina sol–gel matrix dynamics cannot be the origin of these fluctuations, given that the THF samples lack sol–gel. These motions most likely stem from the movements of surrounding THF molecules, which are the major component of the ruthenium complex solvent shells. The shorter time scale dynamics of the surrounding solvent shell do not appear to be modified by confinement in the alumina sol–gel. The similarities in shorter time scale dynamics among the three samples can be rationalized by referring to previous studies conducted by Yamada and co-workers that examined the effects of nanoconfinement on solvent reorientational dynamics in nanoporous silicate sol–gel glasses.[44] In these nanoconfined spaces, the fastest observable solvent motions occurred on time scales similar to bulk solvent motions. These motions were attributed to solvent molecules far enough away from the walls of the pore that they were essentially bulk-like. Conversely, slower solvent dynamics arose from solvent molecules interacting with the surfaces of the silica nanopore. Previous work from our group reported a similar separation of dynamics in silica sol–gel pores into bulk-like and surface-like categories.[45,46] The similarity in τ_1 among the three samples here indicates that the carbonyl groups are sensing solvent molecules that behave like bulk THF rather than those found near the walls of the nanopores.

In the current study, the slower motions of the surroundings, which include the solvent and possibly the alumina backbone, result in variable offsets in the CLS decays in Fig. 4. The magnitude of the CLS offset can be used to identify differences in unresolvably slow inhomogeneous dynamics sensed by the carbonyl ligands among the Ru_3CO_{12} and the free and encapsulated hydrides. For all T_ws beyond 6 ps, the CLS offset is the largest for $[Ru_3CO_{11}H]^-$ in the sol–gel, only slightly smaller for $[Ru_3CO_{11}H]^-$ in THF, and nearly zero for Ru_3CO_{12} in THF. The sol–gel offset exceeding that of the hydride implies that the solvent molecules near the walls of an alumina nanopore and motions of the alumina walls contribute toward slower dynamics. However, the offset of the hydride dissolved in THF differs by less than 10% from the sol–gel, implying that bulk solvent motions are the primary source of the slower dynamics.

The CLS decays were used to quantify the homogeneous and inhomogeneous contributions to the FTIR linewidth via the frequency–frequency correlation function (FFCF).[47] The following correlation function was assumed for the fitting:

$$C(t) = \frac{\delta(t)}{T_2} + \Delta_1^2 e^{\frac{-t}{\tau_1}} + \Delta_0^2,$$

where T_2 is the dephasing time associated with the homogeneous linewidth; Δ_1 and τ_1 are the inhomogeneous amplitude and time constants, respectively; and Δ_0 is the contribution to the linewidth

TABLE I. FFCF fit parameters including VER time constants.

Sample	ν_{CO} (cm^{-1})	T_1 (ps)	Γ (cm^{-1})	Δ_1 (cm^{-1})	τ_1 (ps)	Δ_0 (cm^{-1})
Ru_3CO_{12} in THF	2060.04 (±0.08)	144 (±4)	2.9 (±0.2)	4.57 (±0.03)	2.6 (±0.9)	2.00 (±0.05)
$[Ru_3CO_{11}H]^-$ sol–gel	2014.20 (±0.09)	30 (±4)	1.9 (±0.3)	2.74 (±0.05)	3 (±1)	3.14 (±0.03)
$[Ru_3CO_{11}H]^-$ in THF	2013.90 (±0.07)	37 (±2)	2.1 (±0.2)	3.7 (±0.08)	2.4 (±1)	2.96 (±0.05)

from long time scale inhomogeneous dynamics. T_2 is related to the homogeneous linewidth by $\Gamma = (\pi T_2)^{-1}$; the time constants obtained from the CLS decays are used without adjustment in the $C(t)$, while the amplitudes, Δ_x, are floated to account for inhomogeneity in the linear line shape. The results of the FFCF fitting analysis are shown in Table I.

At the outset, one might expect that the dynamics of the entrapped hydride species would be distinct from those of the hydride in THF and that perhaps $Ru_3(CO)_{12}$ and $[Ru_3CO_{11}H]^-$ in THF would be relatively similar. Indeed, spectral diffusion is usually found to be more reflective of the dynamics in the solvation shell rather than the molecular structure to which the oscillator is attached.[21,48,49] There are also examples in the literature in which encapsulation in sol–gel glasses leads to modification of vibrational dynamics on specific time scales, presumably due to changes in the surrounding solvent or excluded volume effects (guest species partially solvated by the pore wall).[50–52] However, the FFCF analysis of $[Ru_3CO_{11}H]^-$ dissolved in THF and entrapped in a sol–gel shows that this is not always the case.

The FTIR peak widths are relatively insensitive among the three samples, decreasing from 12 to 11 to 10 cm^{-1} for Ru_3CO_{12}, $[Ru_3CO_{11}H]^-$ in THF, and $[Ru_3CO_{11}H]^-$ in the sol–gel, respectively. However, the FFCF analysis reveals that the dynamic contributions to these linewidths do change, as anticipated from the 2D peak shapes in Fig. 3. For $Ru_3(CO)_{12}$ in THF, the homogeneous linewidth (Γ) contributes about 25% of the total FTIR linewidth, while in the sol–gel and synthesized hydride, they contribute about 20%. Therefore, the relative homogeneous contributions to the FTIR linewidth decrease upon conversion to the hydride, while the relative inhomogeneous contributions to the FTIR linewidth (summation of Δ_1 and Δ_0) increase. This suggests the presence of slower overall solvent dynamics for both hydrides compared to Ru_3CO_{12} in bulk THF. If the slowed dynamics were primarily due to confined solvent in the sol–gel pores, the $[Ru_3CO_{11}H]^-$ dissolved in THF would not experience a relative increase in the inhomogeneous linewidth similar to that of the sol–gel. For both hydrides, the measurable spectral diffusion (Δ_1) shrinks, while the static inhomogeneous offset (Δ_0) increases. This offset in the FFCF represents the dynamics that are relatively slow on the time scale of our measurements and appear as static inhomogeneity.

Overall, the dynamic differences between the two hydrides are subtle; they are after all the same molecule in nearly the same solvent. In analyzing these subtleties, we note that complexes near a pore wall would be in closer proximity to slower moving solvent molecules interacting with the pore wall and possibly slow movements of the alumina itself; this would potentially lead to an increase in Δ_0. Concomitantly, some of the CO oscillators on these molecules would be less influenced by the bulk-like motions of solvent molecules near the middle of the pore wall leading to a decrease in Δ_1. In fact, $[Ru_3CO_{11}H]^-$ in the sol–gel is likely to be found near the surfaces of a nanopore and the FFCF parameters for its CO vibrations are consistent with these changes.

The most substantial changes are observed upon conversion from $Ru_3(CO)_{12}$ to $[HRu_3(CO)_{11}]^-$, regardless of whether the hydride is in THF or a sol–gel pore. The fast dynamics captured by Γ get faster for the hydrides. Previous studies have shown that solvent molecules near surfaces exhibit order.[12,13] This molecular order decreases molecular inhomogeneity at the pore surface and, therefore, the inhomogeneous linewidth. Returning momentarily to the VER discussed above, the faster relaxation time of the hydrides contributes to this homogeneous dynamic difference; however, the trend is in the wrong direction and the faster VER should increase Γ rather than decreasing it. Furthermore, for the long relaxation times in Table I, this could be attributed to no more than 0.15 cm^{-1} of the change in Γ. Clearly, these faster homogeneous dynamics of molecules in the hydride solvation shell that perturb the CO frequencies are slowed down. At the same time, the quasi-static dynamics captured by Δ_0 are 50% less for $Ru_3(CO)_{12}$, and a concurrent increase in the 3 ps dynamics is also observed. Thinking of the dynamics as a continuum where the dynamics that are categorized by Γ (fastest), Δ_0 (medium), and Δ_0 (slow), the overall trend is a shift of faster movements in $Ru_3(CO)_{12}$ to slower movements in $[HRu_3(CO)_{11}]^-$.

A pertinent comparison should be made between the hydride results and those in the literature that have shown modified dynamics for charged compounds relative to structurally similar but neutral species.[53,54] Dutta and co-workers reported that charged and neutral azides exhibited different spectral diffusion dynamics with the charged variants displaying significantly slower dynamics, consistent with the charged hydrides in the current work.[53] Similarly, it was shown recently by Kiefer and co-workers that charged organometallic catalysts showed slower spectral diffusion in spectroelectrochemical 2D-IR measurements.[54] In all cases, the operational principle is that the solvation shell structure is modified by the charge state of the analyte, and stronger solute–solvent interactions lead to slower vibrational dynamics. This is a plausible explanation for the observed differences of the hydrides relative to the neutral parent compound. Further work to simulate the solvation shell structure around these two species may shed light on the origins of these changes.

CONCLUSIONS

The ruthenium hydride $[HRu_3(CO)_{11}]^-$ studied in this work experiences fundamentally different dynamics than its parent compound $Ru_3(CO)_{12}$. The accelerated VER shows that the CO vibrations couple more effectively to the surrounding solvent environment for this species, whether dissolved in neat THF or entrapped in an alumina sol–gel matrix. At the same time, the homogeneous and inhomogeneous dynamics that are characterized by 2D-IR line shape analysis report an overall slowing of the frequency fluctuations in the hydride. The dynamic changes experienced by the hydride encapsulated in alumina were found to be small but measurable. This is interesting because the alumina encapsulated complex has been reported as a potent catalyst for alkene hydrogenation reactions, while the parent compound and even silica sol–gel encapsulated compounds are relatively inactive for the same chemistry. In this work, we explored some of the fundamental differences in solvent dynamics that might contribute to this change in reactivity. Although we cannot definitively connect dynamics to reactivity with these measurements alone, we can conclude that the most likely dynamic contributions are experienced upon transformation to the hydride, not encapsulation in the sol–gel. It is certainly true that the ruthenium hydride experiences a new palette of dynamics that perturb the CO ligands on the time scale of chemical reactions. The

subtlety of the dynamic changes upon encapsulation strongly suggests that the new reactivity in the alumina matrix is not due to a dynamic change in the confined solvent pool. Instead, our work shows that it is more likely that the sol–gel environment stabilizes the reactive hydride structure and protects it from degradation.

SUPPLEMENTARY MATERIAL

See the supplementary material for tabulated biexponential fit parameters to vibrational relaxation decays, 2D-IR off-diagonal peak analysis for $Ru_3(CO)_{12}$ in ultradry THF, and FTIR spectrum of $Ru_3(CO)_{12}$ in THF with water added.

ACKNOWLEDGMENTS

The authors gratefully acknowledge partial support from the National Science Foundation under Grant No. CHE-1856589. C.G.P. was supported, in part, by a Newman and Lillian Bortnick Fellowship. J.G.P. was supported, in part, by a Mistletoe Research Fellowship.

AUTHOR DECLARATIONS

Conflict of Interest

The authors have no conflicts to disclose.

Author Contributions

The manuscript was written through contributions of all authors. All authors have given approval to the final version of the manuscript.

DATA AVAILABILITY

The data that support the findings of this study are available from the corresponding author upon reasonable request.

REFERENCES

[1]P. F. Barbara, T. J. Meyer, and M. A. Ratner, "Contemporary issues in electron transfer research," J. Phys. Chem. **100**, 13148–13168 (1996).
[2]O.-H. Kwon, T. H. Yoo, C. M. Othon, J. A. Van Deventer, D. A. Tirrell, and A. H. Zewail, "Hydration dynamics at fluorinated protein surfaces," Proc. Natl. Acad. Sci. U. S. A. **107**, 17101–17106 (2010).
[3]R. M. Stratt and M. Maroncelli, "Nonreactive dynamics in solution: The emerging molecular view of solvation dynamics and vibrational relaxation," J. Phys. Chem. **100**, 12981–12996 (1996).
[4]M. E. Tuckerman, D. Marx, and M. Parrinello, "The nature and transport mechanism of hydrated hydroxide ions in aqueous solution," Nature **417**, 925–929 (2002).
[5]C. P. Casey, S. E. Beetner, and J. B. Johnson, "Spectroscopic determination of hydrogenation rates and intermediates during carbonyl hydrogenation catalyzed by Shvo's hydroxycyclopentadienyl diruthenium hydride agrees with kinetic modeling based on independently measured rates of elementary reactions," J. Am. Chem. Soc. **130**, 2285–2295 (2008).
[6]P. B. Chock and J. Halpern, "Kinetics of the addition of hydrogen, oxygen, and methyl iodide to some square-planar iridium(I) complexes," J. Am. Chem. Soc. **88**, 3511–3514 (1966).
[7]R. Ugo, A. Pasini, A. Fusi, and S. Cenini, "Kinetic investigation of some electronic and steric factors in oxidative addition reactions to Vaska's compound," J. Am. Chem. Soc. **94**, 7364–7370 (1972).
[8]G. Cainelli, P. Galletti, and D. Giacomini, "Solvent effects on stereoselectivity: More than just an environment," Chem. Soc. Rev. **38**, 990–1001 (2009).
[9]J. Gao, "Hybrid quantum and molecular mechanical simulations: An alternative avenue to solvent effects in organic chemistry," Acc. Chem. Res. **29**, 298–305 (1996).
[10]V. Farina, B. Krishnan, D. R. Marshall, and G. P. Roth, "Palladium-catalyzed coupling of arylstannanes with organic sulfonates—A comprehensive study," J. Org. Chem. **58**, 5434–5444 (1993).
[11]P. A. Fitzpatrick and A. M. Klibanov, "How can the solvent affect enzyme enantioselectivity," J. Am. Chem. Soc. **113**, 3166–3171 (1991).
[12]R. Riva, S. Schmeits, C. Jérôme, R. Jérôme, and P. Lecomte, "Combination of ring-opening polymerization and 'click chemistry': Toward functionalization and grafting of poly(epsilon-caprolactone)," Macromolecules **40**, 796–803 (2007).
[13]T. C. Schutt, V. S. Bharadwaj, G. A. Hegde, A. J. Johns, and C. Mark Maupin, "*In silico* insights into the solvation characteristics of the ionic liquid 1-methyltriethoxy-3-ethylimidazolium acetate for cellulosic biomass," Phys. Chem. Chem. Phys. **18**, 23715–23726 (2016).
[14]M. Brunori, F. Cutruzzolà, C. Savino, C. Travaglini-Allocatelli, B. Vallone, and Q. H. Gibson, "Does picosecond protein dynamics have survival value?," Trends Biochem. Sci. **24**, 253–255 (1999).
[15]T. A. Jackson, M. Lim, and P. A. Anfinrud, "Complex nonexponential relaxation in myoglobin after photodissociation of MbCo: Measurement and analysis from 2 ps to 56 *v*s," Chem. Phys. **180**, 131–140 (1994).
[16]K. A. Merchant, W. G. Noid, R. Akiyama, I. J. Finkelstein, A. Goun, B. L. McClain, R. F. Loring, and M. D. Fayer, "Myoglobin-CO substate structures and dynamics: Multidimensional vibrational echoes and molecular dynamics simulations," J. Am. Chem. Soc. **125**, 13804–13818 (2003).
[17]A. Ostermann, R. Waschipky, F. G. Parak, and G. U. Nienhaus, "Ligand binding and conformational motions in myoglobin," Nature **404**, 205–208 (2000).
[18]J. Pu, J. Gao, and D. G. Truhlar, "Multidimensional tunneling, recrossing, and the transmission coefficient for enzymatic reactions," Chem. Rev. **106**, 3140–3169 (2006).
[19]M. Karplus, "Aspects of protein reaction dynamics: Deviations from simple behavior," J. Phys. Chem. B **104**, 11–27 (2000).
[20]B. H. Jones, C. J. Huber, I. C. Spector, A. M. Tabet, R. L. Butler, Y. Hang, and A. M. Massari, "Correlating solvent dynamics and chemical reaction rates using binary solvent mixtures and two-dimensional infrared spectroscopy," J. Chem. Phys. **142**, 212441 (2015).
[21]L. M. Kiefer and K. J. Kubarych, "Solvent-dependent dynamics of a series of rhenium photoactivated catalysts measured with ultrafast 2D-IR," J. Phys. Chem. A **119**, 959–965 (2015).
[22]H. J. Cho, D. Kim, J. Li, D. Su, and B. Xu, "Zeolite-encapsulated Pt nanoparticles for tandem catalysis," J. Am. Chem. Soc. **140**, 13514–13520 (2018).
[23]H. J. Cho, D. Kim, and B. Xu, "Pore size engineering enabled selectivity control in tandem catalytic upgrading of cyclopentanone on zeolite-encapsulated Pt nanoparticles," ACS Catal. **10**, 8850–8859 (2020).
[24]R. Ciriminna, V. Pandarus, R. Delisi, A. Scurria, M. P. Casaletto, F. Giordano, F. Béland, and M. Pagliaro, "Sol–gel encapsulation of Au nanoparticles in hybrid silica improves gold oxidation catalysis," Chem. Cent. J. **10**, 61 (2016).
[25]K. Smith, N. J. Silvernail, K. R. Rodgers, T. E. Elgren, M. Castro, and R. M. Parker, "Sol–gel encapsulated horseradish peroxidase: A catalytic material for peroxidation," J. Am. Chem. Soc. **124**, 4247–4252 (2002).
[26]Z. Zhang, Q. Xiao, and J. Gu, "Effective synthesis of zeolite-encapsulated Ni nanoparticles with excellent catalytic performance for hydrogenation of CO_2 to CH_4," Dalton Trans. **49**, 14771–14775 (2020).
[27]J. Blum and D. Avnir, *Handbook of Sol-Gel Science and Technology. Processing Characterization and Application*, Applications of Sol-Gel Technology Vol. 3 (Kluwer Academic Publishers, Norwell, 2005), pp. 507–550.
[28]N. Eliau, D. Avnir, M. S. Eisen, and J. Blum, "Activation of metal-carbonyl clusters by their encapsulation within alumina sol-gel matrices," J. Sol-Gel Sci. Technol. **35**, 159–167 (2005).
[29]A. C. Marr and P. C. Marr, "Entrapping homogeneous catalysts by sol–gel methods: The bottom-up synthesis of catalysts that recycle and cascade," Dalton Trans. **40**, 20–26 (2011).
[30]R. H. Crabtree, *The Organometallic Chemistry of the Transition Metals*, 5th ed. (John Wiley & Sons, 2009).

[31] C. Lau, S. Ng, G. Jia, and Z. Lin, "Some ruthenium hydride, dihydrogen, and dihydrogen-bonded complexes in catalytic reactions," Coord. Chem. Rev. **251**, 2223–2237 (2007).
[32] H. Nagashima, "Facile hydrogenation of acenapthylenes and azulenes on the face of a triruthenium carbonyl moiety: Discovery of specific reactions on the cluster framework providing unique insight for cluster catalysis," Monatsh. Chem. **131**, 1225–1239 (2000).
[33] J. G. Patrow, Y. Cheng, C. G. Pyles, B. Luo, I. A. Tonks, and A. M. Massari, "Spectroscopic study of sol–gel entrapped triruthenium dodecacarbonyl catalyst reveals hydride formation," J. Phys. Chem. Lett. **11**, 7394–7399 (2020).
[34] G. A. Battiston, G. Bor, U. K. Dietler, S. F. A. Kettle, R. Rossetti, G. Sbrignadello, and P. L. Stanghellini, "Solid-state studies. 20. Comparative infrared and Raman-spectroscopic upsilon-(Co) study of $Ru_3(Co)_{12}$, $Os_3(Co)_{12}$, their mixed-crystals, and the mixed triangulo cluster carbonyls $Ru_2Os(Co)_{12}$ and $RuOs_2(Co)_{12}$," Inorg. Chem. **19**, 1961–1973 (1980).
[35] G. A. Battiston, G. Sbrignadello, and G. Bor, "Infrared spectroscopic studies on metal carbonyl compounds. 23. A simple quantitative treatment of the infrared band intensity and the induced metal-metal dipole contribution to it in polynuclear metal-carbonyls. An application to the spectrum of dodecacarbonyltriruthenium and dodecacarbonyltriosmium in the carbon-oxygen stretching region," Inorg. Chem. **19**, 1973–1977 (1980).
[36] X. Dong, F. Yang, J. Zhao, and J. Wang, "Efficient intramolecular vibrational excitonic energy transfer in $Ru_3(CO)_{12}$ cluster revealed by two-dimensional infrared spectroscopy," J. Phys. Chem. B **122**, 1296–1305 (2018).
[37] B. Sun, G. A. Shi, S. V. Nageswara Rao, M. Stavola, N. H. Tolk, S. K. Dixit, L. C. Feldman, and G. Lüpke, "Vibrational lifetimes and frequency-gap law of hydrogen bending modes in semiconductors," Phys. Rev. Lett. **96**, 035501 (2006).
[38] Y. J. Chabal, A. L. Harris, K. Raghavachari, and J. C. Tully, "Infrared spectroscopy of H-terminated silicon surfaces," Int. J. Mod. Phys. B **7**, 1031–1078 (1993).
[39] J. W. Lyding, K. Hess, and I. C. Kizilyalli, "Reduction of hot electron degradation in metal oxide semiconductor transistors by deuterium processing," Appl. Phys. Lett. **68**, 2526–2528 (1996).
[40] F. F. Crim, "Chemical dynamics of vibrationally excited molecules: Controlling reactions in gases and on surfaces," Proc. Natl. Acad. Sci. U. S. A. **105**, 12654–12661 (2008).
[41] A. Gutiérrez-González, F. F. Crim, and R. D. Beck, "Bond selective dissociation of methane (CH_3D) on the steps and terraces of Pt(211)," J. Chem. Phys. **149**, 074701 (2018).
[42] E. E. Fenn and M. D. Fayer, "Extracting 2D IR frequency-frequency correlation functions from two component systems," J. Chem. Phys. **135**, 074502 (2011).
[43] I. C. Spector, C. M. Olson, C. J. Huber, and A. M. Massari, "Simple fully reflective method of scatter reduction in 2D-IR spectroscopy," Opt. Lett. **40**, 1850–1852 (2015).
[44] S. A. Yamada, J. Y. Shin, W. H. Thompson, and M. D. Fayer, "Water dynamics in nanoporous silica: Ultrafast vibrational spectroscopy and molecular dynamics simulations," J. Phys. Chem. C **123**, 5790–5803 (2019).
[45] C. J. Huber, S. M. Egger, I. C. Spector, A. R. Juelfs, C. L. Haynes, and A. M. Massari, "2D-IR spectroscopy of porous silica nanoparticles: Measuring the distance sensitivity of spectral diffusion," J. Phys. Chem. C **119**, 25135–25144 (2015).
[46] C. J. Huber and A. M. Massari, "Characterizing solvent dynamics in nanoscopic silica sol–gel glass pores by 2D-IR spectroscopy of an intrinsic vibrational probe," J. Phys. Chem. C **118**, 25567–25578 (2014).
[47] K. Kwak, S. Park, I. J. Finkelstein, and M. D. Fayer, "Frequency-frequency correlation functions and apodization in two-dimensional infrared vibrational echo spectroscopy: A new approach," J. Chem. Phys. **127**, 124503 (2007).
[48] C. G. Pyles, C. M. Olson, and A. M. Massari, "Vibrational heavy atom effect controls relaxation and spectral diffusion in triphenyl hydride complexes," Chem. Phys. **512**, 98–103 (2018).
[49] C. M. Olson, A. Grofe, C. J. Huber, I. C. Spector, J. Gao, and A. M. Massari, "Enhanced vibrational solvatochromism and spectral diffusion by electron rich substituents on small molecule silanes," J. Chem. Phys. **147**, 124302 (2017).
[50] A. M. Massari, I. J. Finkelstein, and M. D. Fayer, "Dynamics of proteins encapsulated in silica sol–gel glasses studied with IR vibrational echo spectroscopy," J. Am. Chem. Soc. **128**, 3990–3997 (2006).
[51] R. A. Farrer and J. T. Fourkas, "Orientational dynamics of liquids confined in nanoporous sol–gel glasses studied by optical Kerr effect spectroscopy," Acc. Chem. Res. **36**, 605–612 (2003).
[52] U. Narang, R. Wang, P. N. Prasad, and F. V. Bright, "Effects of aging on the dynamics of rhodamine-6G in tetramethyl orthosilicate-derived sol-gels," J. Phys. Chem. **98**, 17–22 (1994).
[53] S. Dutta, Z. Ren, T. Brinzer, and S. Garrett-Roe, "Two-dimensional ultrafast vibrational spectroscopy of azides in ionic liquids reveals solute-specific solvation," Phys. Chem. Chem. Phys. **17**, 26575–26579 (2015).
[54] L. M. Kiefer, L. B. Michocki, and K. J. Kubarych, "Transmission mode 2D-IR spectroelectrochemistry of *in situ* electrocatalytic intermediates," J. Phys. Chem. Lett. **12**, 3712–3717 (2021).